INTERACTION OF LASER RADIATION WITH MATTER

PACS numbers: 42.68.Jg;42.68.Ge;42.65.-k
DOI: 10.1070/QE2006v036n04ABEH013152

Clearing of a polydisperse water aerosol by a laser pulse in the diffusive – convective regime

A.N. Kucherov

***Abstract*. The propagation of an IR laser pulse through a water aerosol layer (fog, clouds) is studied. The relative motion of the beam and medium, the diffraction spread, thermal self-action of the laser beam, absorption and scattering of radiation by particles, evaporation of particles (aerosol clearing), and the size distribution of particles were taken into account. The propagation problem was solved numerically at a macroscopic scale of the order of the beam transverse size, and the action of radiation on drops was considered at a microscopic scale of the order of the particle radius. A satisfactory agreement was obtained between theoretical and experimental results.**

Keywords: *laser beam, spherical drops, evaporation, medium clearing*.

1. Introduction

The problem of a water aerosol clearing by a laser beam is studied by introducing two scales: the transverse size of the laser beam $r_0 \sim 10^{-3} - 10^{-2}$ m (macroscale) and the characteristic radius of aerosol drops $a \sim 10^{-6}$ m (microscale) [1 – 3]. Of interest is the IR laser radiation range in which transparency windows in air are present [4, 5]. For typical visibility levels $w \sim 10^{-5} - 10^{-4}$ kg m^{-3} (the condensate mass per unit volume) [6], a laser pulse of a relatively low power (~ 1 kW) allows one to reduce considerably the optical thickness of a medium during a short time of the order of the pulse duration, to transmit a probe beam through a clearing channel and to perform remote sensing or optical communication. A complex many-parametric clearing problem is solved, as a rule, by using substantial (and not always correct) simplifications: a fraction of energy absorbed by a drop, which is spent for its evaporation, is assumed constant or preliminary known from estimates of the functions of other quantities; simplified dependences of the radiation absorption and attenuation coefficients on the medium parameters are used; and the effect of an aerosol medium is described with the help of a macroscopically smooth water content function $w(x, y, z, t)$ (water content approximation).

In this paper, the absorption and scattering coefficients were calculated by using the Mie theory [7], the size and temperature of particles and the size distribution of particles were calculated by the finite difference method, the parabolic equation of the beam propagation was solved by the Fourier series expansion method, and a fraction of the absorbed energy spent for drop evaporation was calculated at each step (in time and coordinates). Depending on the intensity of radiation heating a drop (on the Mach number for the vapour velocity on the external boundary of the Knudsen layer), there exist the following regimes of the drop evaporation and destruction: diffusive, diffusive – convective, subsonic, sonic, and explosive [8]. In this paper, the clearing process is studied for moderate evaporation rates from drop surfaces (diffusive and diffusive – convective regimes). Note that high-rate evaporation regimes begin at temperatures close to the boiling temperature [8].

2. Formulation of the problem

The equation describing the propagation of laser radiation in an absorbing and scattering aerosol medium at the macroscopic scale for the slowly varying electric-field amplitude E (the intensity is $I = EE^*$) can be written in the form [9]

$$-2\mathrm{i}kn_0\frac{\partial E}{\partial z} + \frac{\partial^2 E}{\partial x^2} + \left[2k^2 n_0(n_0 - 1) \times \frac{\rho - \rho_0}{\rho_0}E - \mathrm{i}(\alpha_\mathrm{g} + \alpha)kn_0 E\right] = 0, \quad (1)$$

$$E|_{z=0} = E_0(x), \quad E|_{x\to\pm\infty} \to 0, \quad (2)$$

$$h_0\left[\frac{\partial(\rho - \rho_0)}{\partial t} + V_0\frac{\partial(\rho - \rho_0)}{\partial x}\right] = -\alpha_\mathrm{g} I - \alpha_\mathrm{eff} I, \quad (3)$$

$$\rho|_{t=0} = \rho_0, \quad \rho|_{x\to-\infty} \to \rho_0. \quad (4)$$

Here, z is the longitudinal coordinate; x is the coordinate perpendicular to the beam; t is time; $k = 2\pi/\lambda$ is the wave number; n_0 is the refractive index of an unperturbed gas; ρ and ρ_0 are the gas density and its initial unperturbed value; h_0 is the enthalpy of an unperturbed gas; V_0 is the velocity of a transverse flow; α is the linear coefficient of radiation attenuation by the aerosol; $\alpha_\mathrm{eff} = \alpha_\mathrm{abs}\eta$ is the effective

A.N. Kucherov N.E. Zhukovskii Central Aerohydrodynamic Institute (TsAGI), ul. Zhukovskogo 1, 140180 Zhukovskii, Moscow region, Russia; e-mail: ank@aerocentr.msk.su

Received 19 September 2005; revision received 30 November 2005
Kvantovaya Elektronika **36** (4) 363 – 368 (2006)
Translated by M.N. Sapozhnikov

radiation absorption coefficient by the gas; α_g, α_{abs} are the absorption coefficients of the gas and aerosol; and η is the fraction of energy absorbed by the aerosol escaping to the gas.

Without the loss of generality, consider a plane beam with the initial Gaussian transverse intensity distribution $E_0(x) = \sqrt{I_0}\exp[-(x/r_0)^2/2]$, where $I_0 = P_0/\pi r_0^2$ is the characteristic radiation intensity; P_0 is the total power; and r_0 is the beam radius. The absorption and attenuation coefficients of the aerosol are [6, 7]

$$\alpha(x,z,t) = \pi N\int_0^\infty a^2 Q_{ext}(a)f(a)\mathrm{d}a, \quad \beta = \frac{\alpha}{w}, \tag{5}$$

$$\alpha_{abs}(x,z,t) = \pi N\int_0^\infty a^2 Q_{abs}(a)f(a)\mathrm{d}a, \quad \beta_{abs} = \frac{\alpha_{abs}}{w}, \tag{6}$$

$$\alpha_{eff}(x,z,t) = \pi N\int_0^\infty a^2 Q_{abs}(a)\eta_a f(a)\mathrm{d}a = \alpha_{abs}\eta,$$

$$w(x,z,t) = \frac{4\pi N\rho_w}{3}\int_0^\infty a^3 f(a)\mathrm{d}a.$$

Here, β_{abs} and β are the specific (per unit mass) absorption and attenuation coefficients of the aerosol; w is the water content (moisture function) of the aerosol; $\eta_a = j_T S/Q_{abs}\sigma I = 4j_T/Q_{abs}I$ is the fraction of heat losses to a gas of the energy absorbed in a particle; $S = 4\pi a^2$ and $\sigma = \pi a^2$ are the total area and area of the sphere cross section, respectively; N is the number of particles per unit volume; Q_{ext} is the radiation attenuation (extinction) factor in a sphere of radius a; and $f(a)$ is the size (radius) distribution function of particles.

Variations in the drop radius a, its temperature T, and the size distribution f of particles at the drop microscale are described by the equations [1, 2]

$$\frac{\partial a}{\partial t} + V_0\frac{\partial a}{\partial x} = -\frac{j}{\rho_w}, \quad a|_{t=0} = a_0, \tag{7}$$

$$\rho_w C_w\left(\frac{\partial T}{\partial t} + V_0\frac{\partial T}{\partial x}\right) = \alpha_d I(x,z,t)$$

$$-\frac{3}{a}(jH_w + j_T), \quad T|_{t=0} = T_\infty, \tag{8}$$

$$\frac{\partial f}{\partial t} + V_0\frac{\partial f}{\partial x} + \frac{\partial}{\partial a}\left(f\frac{\mathrm{d}a}{\mathrm{d}t}\right) = 0,$$

$$f|_{t=0} = f_0(a_0) \equiv \frac{\mu^{\mu+1}a_0^\mu}{\Gamma(\mu+1)a_m^{\mu+1}}\exp\left(-\mu\frac{a_0}{a_m}\right). \tag{9}$$

Here, j (kg m^{-2} s^{-1}) and j_T (W m^{-2}) are the densities of mass and thermal fluxes from the drop surface; ρ_w (kg m^{-3}) and C_w (J kg^{-1} K^{-1}) are the density and specific heat of water, respectively; H_w (J kg^{-1}) is the specific heat of evaporation; a_0 and T_∞ are the initial radius of the drop and its temperature equal to that of the environment; $\alpha_d = 3Q_{abs}/4a$ is the volume-averaged absorption coefficient of the drop; Q_{abs} is the absorption factor of the drop of radius a; $f_0(a_0)$ is the initial size distribution of particles taken in the form of a two-parametric gamma distribution with the parameters μ and a_m [a_m is the modal (most probable) radius]. The mass and heat flows from the drop surfaces have the form

$$j = \begin{cases} \dfrac{\langle\rho D\rangle}{a}\ln\left(\dfrac{1-Y_\infty}{1-Y}\right), & T < T_b, \\ \rho_K u_K, & T \geqslant T_b, \end{cases} \tag{10}$$

$$Y_\infty = \frac{p_{s\infty}m_v}{p_\infty m},$$

$$j_T = \begin{cases} -\langle k\rangle\left.\dfrac{\partial T}{\partial r}\right|_{r=a} = j\langle k\rangle\left\langle\dfrac{C_p}{k}\right\rangle\dfrac{T-T_\infty}{e^{(ja\langle C_p/k\rangle)}-1}, & T < T_b, \\ \rho_K u_K\left[h_K(T_K) - h_s(T) + \dfrac{u_K^2}{2}\right], & T \geqslant T_b. \end{cases} \tag{11}$$

Here, the angle brackets mean averaging over the temperature range of thermal characteristics: the diffusion coefficient D of vapour, the specific heat C_p of the gas and the heat conductivity coefficient k of air; $Y = \rho_v/\rho$ and Y_∞ are the relative mass concentration of vapour and its value in surrounding air, respectively; ρ_v is the vapour density; ρ is the density of the air–vapour mixture; $p_{s\infty}$ and p_∞ are the pressures of the saturated vapour and air at temperature T_∞, respectively; m_v and m are the molar masses of vapour and air; ρ_K and u_K are the vapour density and velocity at the external boundary of the Knudsen layer, respectively [10]; $h_s(T)$ and $h_K(T_K)$ are the enthalpy of vapour saturated at the drop-surface temperature T and the enthalpy of vapour at the upper boundary of the Knudsen layer, respectively. The temperature T_b, close to the boiling temperature, separates slow and rapid evaporation regimes. Variations in the quantities over the entire temperature range of the drop, from the initial value T_∞ to the critical value (647.3 K) were analysed in [8].

The propagation equation (1) was solved by the method of expansion in a Fourier series using the fast Fourier transform [11], the drop heating and evaporation equations, and the evolution equation for the size distribution function of particles, which was solved with the help of the second-order finite difference McCormack scheme of approximation over time and coordinate [12, 13].

Let us introduce dimensionless quantities into equations by dividing the coordinate z by the path length L, the coordinate x by the initial radius r_0, time t by the characteristic value $t_0 = r_0/V_0$, the function of the field E by $\sqrt{I_0}$, the particle radius by a_m, temperature by T_∞, the size distribution function of particles by $f_m = f_0(a_m)$, the moisture function by w_0, and the coefficients α_g, α, and α_{eff} by their characteristic values α_{g0}, α_0, and $\alpha_{eff\,0}$:

$$\alpha_{g0} = \alpha_g(T_\infty), \ \alpha_0 = \pi N a_m^2 Q_{ext}(a_m),$$

$$\alpha_{eff\,0} = \eta_0\pi N a_m^2 Q_{abs}(a_m).$$

The similarity parameters in (1) are the Fresnel number $F = kn_0 r_0^2/L$, the parameters of radiation attenuation by the gas ($N_g = \alpha_{g0}L$) and aerosol ($N_\beta = \alpha_0 L$), and the thermal self-action (self-refraction) parameter $N_T = (L/L_T)^2$, where $L_T = r_0/[Q(n_0-1)/n_0]^{1/2}$ is the thermal self-action length (the length of an essential change in the beam diameter caused by the medium heating and the refractive index change), and $Q = \alpha_{eff\,0}I_0 t_0/\rho_0 h_0$.

The right-hand part of heating equation (8) contains the parameters

$$Q_I = \frac{\alpha_{\rm dm} I_0 t_0}{\rho_{\rm w} C_{\rm w} T_\infty},\ Q_H = \frac{j_0 H_\infty t_0}{a_{\rm m} \rho_{\rm w} C_{\rm w} T_\infty},$$

$$Q_{jT} = \frac{j_{T0} t_0}{a_{\rm m} \rho_{\rm w} C_{\rm w} T_\infty}$$

[where $\alpha_{\rm dm} = \alpha_{\rm d}(a_{\rm m})$; $H_\infty = H_{\rm w}(T_\infty)$; j_0, j_{T0} are the characteristic values] which determine the heat supply efficiency, evaporation expenditure, and heat losses through the drop surface, respectively. Estimates and solutions of Eqns (7) and (8) show that drops are heated for the shorter time $\Delta t \sim t_0/Q_I$ than the time of their evaporation which occurs upon a slow decrease in their temperature under the condition that $dT/dt \approx 0$ or $Q_I \sim Q_H + Q_{jT}$. The clearing efficiency determines the evaporation efficiency or the evaporation parameter $\eta_{\rm v} = jH_{\rm w}/(jH_{\rm w} + j_T)$ [1, 2, 14]. For $dT/dt \approx 0$, we have $\eta_{\rm v} = 1 - \eta_{\rm a}$. Let us set $Q_I = 3(Q_H + Q_{jT})$ and introduce the characteristic efficiency $\eta_{\rm v0} = j_0 H_\infty/(j_0 H_\infty + j_{T0})$, where $j_0 = \alpha_{\rm dm} I_0 a_{\rm m} \eta_{\rm v0}/3H_\infty$ and $j_{T0} = j_0 H_\infty (1 - \eta_{\rm v0})/\eta_{\rm v0}$.

Because the absorption parameter $N_{\rm g}$ of the gas is small for short paths ($L < 10^2$ m), we set $N_{\rm g} \equiv 0$.

Equations (7) and (9) contain the dimensionless parameter

$$N_{\rm v0} = \frac{\alpha_{\rm dm} I_0 \eta_{\rm v0} r_0}{3\rho_{\rm w} H_{\rm w} V_0}, \tag{12}$$

which characterises the efficiency (velocity, strength) of the drop decrease and, therefore, of the clearing process. This is a microscopic parameter. More accurately, the clearing process at the macroscale of the beam radius r_0 is characterised by the integral parameter

$$N_{\rm v} = \int_0^\infty \frac{\alpha_{\rm d}(a)\eta_{\rm v}(a) I_0 r_0}{3\rho_{\rm w} H_{\rm w} V_0} f(a)\,{\rm d}a. \tag{13}$$

The parameter $N_{\rm v}$ will be needed in the future to compare the results with the moisture function approximation. The absorption coefficient $\alpha_{\rm d}$ and the evaporation parameter $\eta_{\rm v}$ depend on the drop radius a and considerably vary in time and over coordinates. It is more convenient to use the fixed, independent of coordinates, clearing parameter $N_{\rm v0}$. Also, some characteristic constant value $\eta_{\rm v0}$ can be used, for example,

$$\eta_{\rm v,min} = \left[1 + \frac{k_\infty T_\infty^2 m p_{\infty} R}{\rho_\infty D_\infty H_\infty^2 m_{\rm v}^2 p_{\rm s\infty}}\right]^{-1}$$

(the lower limit of diffusion evaporation) or a value known from estimates if the temperature and pressure of the surrounding air and other parameters vary. Bleaching results in a decrease in the optical thickness of an aerosol layer

$$\tau(x, z, t) = \int_0^z \alpha\,{\rm d}z. \tag{14}$$

Instead of the attenuation parameter N_β of the aerosol, the equivalent parameter differing in a constant factor – the initial optical thickness $\tau_0 = \tau(x = 0, L, t = 0)$ can be used.

The cells of the calculation network used for numerical solution were $\Delta t = 10^{-4} - 10^{-3}$, $\Delta x = 0.1$ (the number of grid nodes was $N_x = 64$), $\Delta z = 0.04$ ($N_z = 25$), $\Delta a = 0.1 a_{\rm m}$ ($N_{\rm a} = 40$). The vapour mass and thermal fluxes from a drop surface were calculated to the temperature $T_{\rm b}$ (close to the boiling point) and after its achievement, from expressions for the diffusive–convective and subsonic regimes (in the limit, sonic) regimes using interpolation in the intermediate interval. In this paper, we analyse the results obtained for the diffusive–convective evaporation regime.

3. The main results

Consider several variants differing considerably in the pressure and temperature of the surrounding air.

Variant I. At the atmospheric pressure of the environment $p_\infty = 1.01325 \times 10^5$ Pa and temperature $T_\infty = 293.15$ K (the air density is $\rho_\infty = 1.225$ kg m^{-3}, the saturated vapour pressure is $p_{\rm s\infty} = 2.337 \times 10^3$ Pa or the relative pressure parameter of saturated vapour $N_p = p_{\rm s\infty}/p_\infty = 2.30 \times 10^{-2}$ and $T_{\rm b} = 373$ K), we consider a uniform water aerosol with the number of particles $N = 10^8$ m^{-3} per unit volume, the modal drop radius $a_{\rm m} = 5$ μm, the initial Khrgian–Mazin distribution $\mu = 2$ and, therefore, with the initial water content $w(x, z, t = 0) \equiv w_0 = 3.14 \times 10^{-4}$ kg m^{-3}. We assume in the numerical solution that $a \subset [a_{\rm min}, a_{\rm max}]$, where $a_{\rm min} = 0.1 a_{\rm m} = 0.5$ μm, and $a_{\rm max} = 3.9 a_{\rm m} = 19.5$ μm.

Variant II. Pressure $p_\infty = 0.89876 \times 10^5$ Pa, $T_\infty = 281.65$ K (the air density is $\rho_\infty = 1.11$ kg m^{-3}, saturated vapour pressure $p_{\rm s_\infty} = 1.1916 \times 10^3$ Pa, $N_p = 0.01326$, $T_{\rm b} = 369.7$ K). Here and in variants III and IV, the other physical parameters are the same as for variant I.

Variant III. Pressure $p_\infty = 5.0535 \times 10^4$ Pa, temperature $T_\infty = 252.38$ K ($\rho_\infty = 0.697$ kg m^{-3}, $p_{\rm s_\infty} = 167$ Pa, $N_p = 2.378 \times 10^{-4}$, $T_{\rm b} = 354.8$ K).

Variant IV. Pressure $p_\infty = 0.0756 \times 10^5$ Pa, temperature $T_\infty = 216.66$ K ($\rho_\infty = 0.12159$ kg m^{-3}, $p_{\rm s_\infty} = 4.00$ Pa, $N_p = 5.291 \times 10^{-4}$, $T_{\rm b} = 313.6$ K).

We assume that $N_\beta = 0.1$ ($\tau_0 = 0.5664$), $N_T = 0, 1$, $N_{\rm v0} = 1$, the radiation wavelength is 10.6 μm [then $Q_{\rm abs}(a_{\rm m}) = 0.524$, $Q_{\rm ext}(a_{\rm m}) = 0.972$, $\alpha_{\rm dm} = 7.86 \times 10^4$ m^{-1}, $\alpha_0 = 7.64 \times 10^{-3}$ m^{-1}, $\alpha_{\rm eff\,0} = 2.06 \times 10^{-3}$ m^{-1}, $L = 13.09$ m] the beam power is $P_0 = 1$ kW ($r_0 = 0.0234$ m, $V_0 = 0.0726$ m s^{-1}, $t_0 = 0.323$ s, $I_0 = 5.80 \times 10^5$ W m^{-2}, and the characteristic pulse energy is $E_0 = P_0 t_0 = 323$ J).

Figure 1a shows the dependence of the drop radius on time t and the longitudinal coordinate z along the path and transverse coordinate x (at the instant $t/t_0 = 1.5$). Figure 1b shows variations in the drop temperature on passing from small drops (of minimum diameter 0.5 μm) to large drops (of maximum diameter 19.5 μm) along the path z for a drop with the initial diameter equal to the maximum diameter $a_0 = 19.5$ μm and also with time t. Typically, the drop temperature rapidly achieves its maximum during the characteristic time $\Delta t/t_0 \sim \alpha_{\rm dm} I_0/\rho_{\rm w} C_{\rm w} T_\infty = 1/Q_I$ (in our example, $T_{\max} = 313$ K) and the drop slowly cools off and its size decreases with the characteristic time $\Delta t/t_0 \sim \rho_{\rm w} a_{\rm m}/t_0 j_0 = 3\rho_{\rm w} H_\infty/(\alpha_{\rm dm} I_0 t_0 \eta_{\rm v0}) = 1/N_{\rm v0}$ [curve (*4*)]. Figure 1c presents the size distributions $f(a)$ of drops at the beam centre ($x = 0$) at different instants.

Figure 2 shows the transverse radiation intensity distributions obtained at different instants after the propagation of radiation through an aerosol layer of

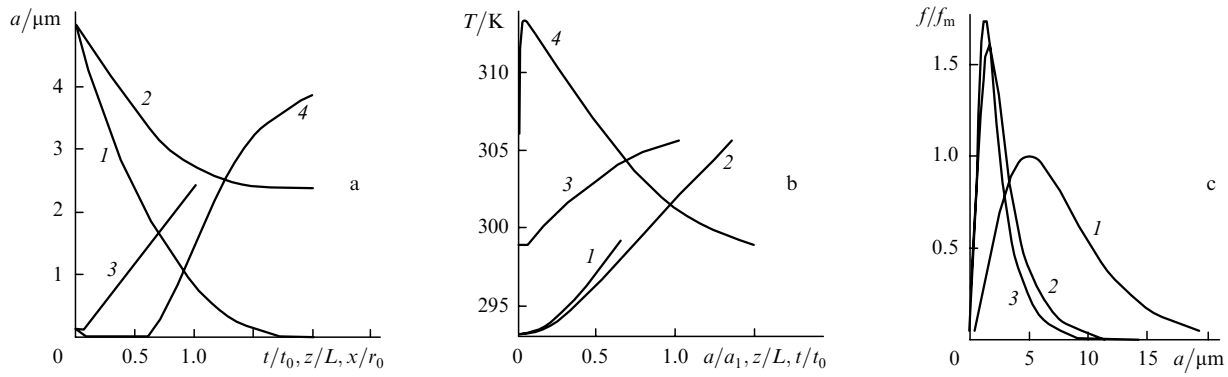

Figure 1. Variations in the drop radius with time t for $z = 0$ (*1*), $z = L$, $a_0 = 5$ μm (*2*) along the path z for $t/t_0 = 1.5$, $x = 0$ (*3*) and along the transverse coordinate x for $z = 0$, $t/t_0 = 1.5$ (*4*) (a); variations in the drop temperature on passing from small to large drops for $z = 0$ (*1*), $z = L$, $t/t_0 = 1.5$, $x = 0$ (*2*), along the path z for $a_0 = 19.5$ μm, $t/t_0 = 1.5$, $x = 0$ (*3*) and with time t for $a_0 = 19.5$ μm, $z = 0$, $x = 0$ (*4*), $a_1 = 10$ μm (b); and the distribution $f(a)$ of particles over their radius at instants $t/t_0 = 0$ (*1*), 1.0 (*2*), and 2.0 (*3*) (coordinates $x = 0$, $z = L$) (c). The results are presented for variant I: the beam power is $P_0 = 10^3$ W, the wavelength is 10.6 μm, the modal radius is $a_m = 5$ μm, the parameter $\mu = 2$, the initial moisture is $w_0 = 3.14 \times 10^{-4}$ kg m^{-3}, the path length is $L = 13.09$ m. The similarity parameters are $N_\beta = 0.1(\tau_0 = 0.5664)$, $N_T = 0.1$, $N_{v0} = 1$, $N_p = 2.30 \times 10^{-2}$, $F = 24.8 \gg 1$.

thickness $L = 13.09$ m and the transverse distributions of the optical thickness $\tau(x, L, t)$. Thermal self-action was taken into account ($N_T = 0.1$), but it was small, as our analysis has shown. Noticeable differences from the case $N_T = 0$ were observed for $N_T \geqslant 0.2$.

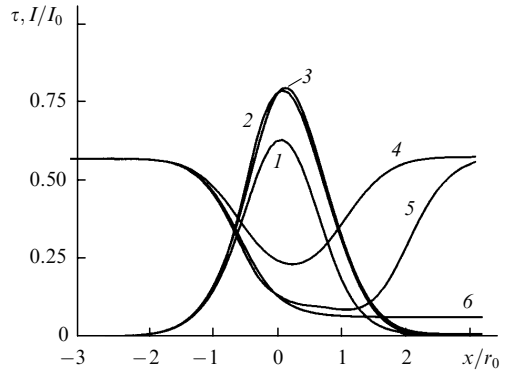

Figure 2. Transverse distributions of the laser radiation intensity I transmitted through an aerosol layer of thickness L (*1–3*) and of the optical thickness τ (*4–6*) at instants $t/t_0 = 0.5$ (*1*, *4*), 1.5 (*2*, *5*) and ∞ (*3*, *6*) for the similarity parameters $N_\beta = 0.1$, $N_T = 0.1$, $N_{v0} = 1$, $F \gg 1$ and $N_p = 2.30 \times 10^{-2}$ (variant I).

The results presented in Fig. 3 were obtained in the ranges of similarity parameters $N_\beta = 0 - 0.5$ ($\tau_0 = 0 - 2.832$) and $N_{v0} = 0 - 2$. Preliminary, a few variants of numerical algorithms and programs were developed for constructing the solution for the total system of equations under nonstationary conditions and in the stationary limit both for relatively small and large variations in the drop temperature. For example, two algorithms were realised in the stationary limit. One of them uses an explicit scheme with a very small step over x $\Delta x/r_0 = 0.00625$ to obtain the solutions of Eqns (1)–(11). Another algorithm uses large steps over the coordinate x ($\Delta x/r_0 = 0.1$) and performs iterations at each step. The results were in agreement within the error less than 1 %. Under nonstationary conditions, the error could achieve 10 %.

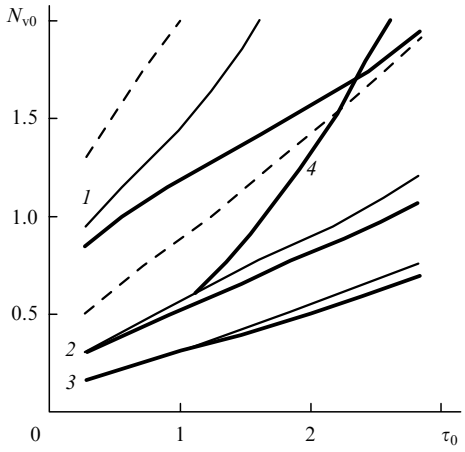

Figure 3. Levels of the optical thickness decrease $\Delta\tau/\tau_0 = (\tau_0 - \tau_{min})/\tau_0 = 0.9$ (*1*), 0.7 (*2*), and 0.5 (*3*) at instants $t/t_0 = 1$ (dashed curves), 2.0 (solid curves) and ∞ (thick curves) in the $\tau_0 - N_{v0}$ (initial optical thickness–clearing parameter) plane of similarity parameters for $N_T = 0.1$, $F \gg 1$, $N_p = 2.30 \times 10^{-2}$ (variant I). Curve (*4*) corresponds to $\Delta\tau/\tau_0 = 0.3$, variant III ($N_p = 2.378 \times 10^{-3}$, $t/t_0 = \infty$).

For variant I, the levels of radiation transmission (transparency levels) $\mathrm{Tr} = I(x = 0, z = L, t)/I_0 = 0.9$, 0.7, 0.5, 0.3, 0.1 were obtained in the plane of similarity parameters $\tau_0 - N_{v0}$ (for $N_T = 0.1$) at different instants of time and in the stationary limit $t/t_0 = \infty$. The curves are similar to those presented in Fig. 3 from [3] for the moisture function approximation. Note that the calculation error increases with decreasing parameters τ_0 and N_{v0}. Some data are presented in Table 1.

Figure 3 shows the levels of decreasing the optical density $\Delta\tau/\tau_0$ at different instants t/t_0 and in the stationary limit $t/t_0 = \infty$.

Table 2 compares the results on the clearing of an aerosol layer of the same optical thickness τ_0 by a 1-kW laser beam obtained for variants I and II for the same parameters N_T and N_{v0} and different values of N_p. The differences in the medium transparency and optical density increase with increasing τ_0 and exceed 15 % for $\tau_0 \approx 1.7$ when N_p decreases by a factor of 1.73.

Table 1. Transparency of the clearing medium $\mathrm{Tr} = I(x = 0, z = L)/I_0$ at the beam centre at the path end for variant I ($N_p = 2.30 \times 10^{-2}$).

τ_0	N_{vo}	t/t_0		
		0.5	1.5	∞
1.133	1	0.277	0.500	0.504
	2	0.531	0.726	0.786
2.266	1	0.0356	0.0920	0.0948
	2	0.105	0.391	0.394
2.833	1	0.0118	0.0323	0.0337
	2	0.0371	0.188	0.192

Table 2. Transparency of the medium $\mathrm{Tr} = I(x = 0, z = L)/I_0$ at the beam centre at the path end and relative changes in the optical thickness $\Delta\tau/\tau_0 = (\tau_0 - \tau_{\mathrm{mig}})/\tau_0$ of the aerosol in the stationary limit for variants I ($N_p = 2.30 \times 10^{-2}$) and II ($N_p = 1.326 \times 10^{-2}$); $P_0 = 1$ kW, $N_T = 0.1$, $N_{\mathrm{v0}} = 0.3$.

Variant	τ_0	Tr	$\Delta\tau/\tau_0$
I	0.5664	0.476	0.608
II		0.468	0.571
I	1.133	0.177	0.459
II		0.165	0.402
I	1.699	0.0608	0.351
II		0.0556	0.300

Table 3 presents the intensity levels of radiation transmitted through the aerosol at the beam centre and the maximum decrease in the optical density of the aerosol over the beam cross section for variants I and III ($N_p \approx 2.38 \times 10^{-3}$). Upon variation in N_p by an order of magnitude, the difference between these variants exceeds 100 %. Finally, Table 4 compares the transparency and optical density of the aerosol in the beam for variants I and IV (for $N_p \approx 5.3 \times 10^{-4}$, which is two orders of magnitude lower than for variant I). The transparency characteristics of the clearing channel in variant IV presented in Table 4 prove to be almost an order of magnitude lower than those in initial variant I. The results for variants I–IV presented in Fig. 3 and Tables 2–4 demonstrate a substantial role of the parameter $N_p = p_{\mathrm{s}_\infty}/p_\infty$, which depends on the environment temperature T_∞ and pressure p_∞.

Table 3. Transparency of the medium $\mathrm{Tr} = I(x = 0, z = L)/I_0$ at the beam centre at the path end and relative changes in the optical thickness $\Delta\tau/\tau_0$ of the aerosol in the stationary limit for variants I and III ($N_p = 2.378 \times 10^{-3}$); $P_0 = 1$ kW, $N_T = 0.1$, $N_{\mathrm{v0}} = 2$.

Variant	τ_0	Tr	$\Delta\tau/\tau_0$
I	1.133	0.755	0.928
III		0.256	0.684
I	1.699	0.562	0.924
III		0.0786	0.482
I	2.266	0.328	0.918
III		0.0243	0.358

The temperature of drops in all the situations considered did not exceed T_b, i.e., evaporation occurred in the diffusive–convective regime. For $N_T \geqslant 0.1$, the high-rate evaporation regimes are realised, which are not considered in this paper. Note that the effect of thermal self-action is negligible. For $N_T > 0.2$, the radiation intensity profile noticeably shifts toward the gas flow, but the value of $\Delta\tau/\tau_0$ for $N_T = 0.2$ changes weakly. The diffraction broadening of the beam did not play any significant role when the Fresnel number was $F \gg 1$.

Table 4. Transparency of the medium $\mathrm{Tr} = I(x = 0, z = L)/I_0$ and relative changes in the optical thickness $\Delta\tau/\tau_0$ of the aerosol layer in the stationary limit for variants I and IV ($N_p = 5.29 \times 10^{-4}$); $P_0 = 1$ kW, $N_T = 0.1$, $\tau_0 = 0.5664$.

Variant	N_{v0}	Tr	$\Delta\tau/\tau_0$
I	1	0.763	0.901
IV		0.336	0.0948
I	2	0.890	0.930
IV		0.338	0.0988
I	3	0.913	0.933
IV		0.341	0.1181

Note that to provide a complete similarity of the situations under study, it is not sufficient to keep the values of N_T, N_β, N_{v0} and N_p constant. There also exist other microscopic parameters of the problem affecting the result; for example, clearing depends on the wavelength or the diffraction parameter $2\pi a/\lambda$. In addition, parameters related to the initial size distribution of drops and the initial drop radius also influence the result, although less strongly. At the same time, it is found that at the constant parameters N_T, N_β, N_{v0} and N_p, variations in the water content w_0, the number of particles per unit volume, and the path length L have no effect on the result. However, variations in the beam power have a noticeable effect.

4. Comparison with experiments

Let us compare the results of calculations with experimental data [1]. The experiments were performed with a 10.6-μm, 800-W CO_2 laser with the beam diameter $2r_0 = 40$ mm in a 4-m thick aerosol layer moving in the perpendicular direction at a speed of 30 cm s^{-1} [15]. The narrow (2 × 2 mm) 0.57-μm probe beam from a DRSh-100 mercury lamp was directed across the region being bleached in the propagation direction of the medium. The radiation collected with a lens was incident on a FEU-69 photomultiplier. Measurements were performed for the optical

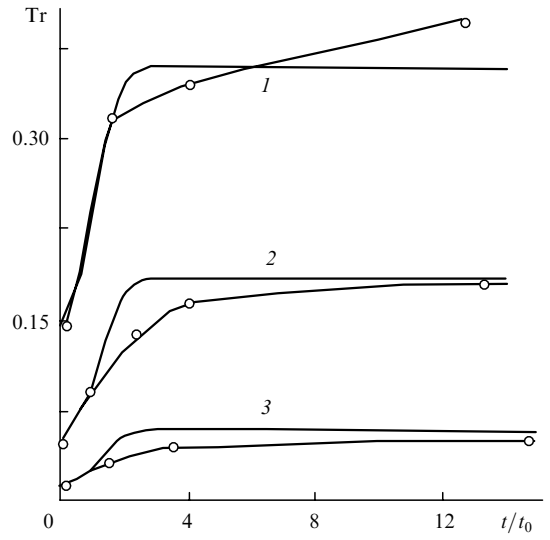

Figure 4. Dependences of the transparency of the 4-m thick aerosol layer $\mathrm{Tr} = I(x = r_0, z = L, t)/I(r_0, 0, t)$ on time t at a wavelength of 0.57 μm for initial optical thicknesses $\tau_0 = 1.91$ (*1*), 2.95 (*2*), and 4.27 (*3*). Points are experiment [1, 15].

thickness of the layer $\tau = 0.2 - 2.8$ at the wavelength 10.6 μm of the clearing beam or $\tau_0 = 1.02 - 6.57$ at the wavelength 0.57 μm of the probe radiation.

Figure 4 presents the time dependences of the transparency function $\mathrm{Tr} = I(x = r_0, L, t)/I(r_0, 0, t)$ of probe radiation for different initial optical thicknesses. One can see that agreement with experimental points is satisfactory. Figure 5 shows the dependences of the transparency function Tr in the stationary limit for large values of t in the entire above-mentioned range of the initial optical densities of the aerosol. It should be expected that the results will considerably improve with increasing the clearing parameter N_{v0}. The transparency functions at the distance of the exponential radius of the beam and variations in the optical thickness at the wavelengths 10.6 and 0.57 μm presented in Table 5 show that the characteristics of the clearing region can be significantly improved only by changing the beam radius and the flow velocity of the medium.

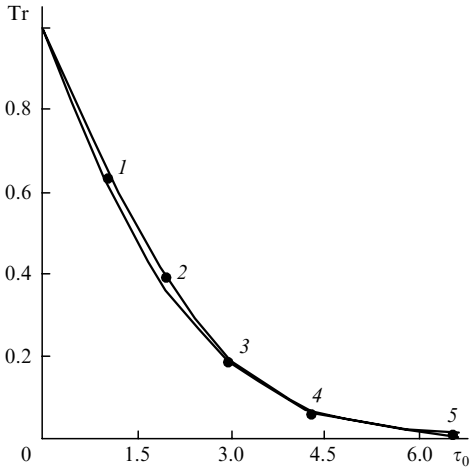

Figure 5. Transparency Tr of the aerosol layer in the stationary limit as a function of the initial optical thickness τ_0. Experimental points (*1–5*) [1, 15] were obtained for $a_m = 1.75$, $\mu = 5$, $\tau_{0\,(10.6)} = 0.206$ (1.02 for $\lambda = 0.57$ μm) (*1*), $a_m = 1.75$, $\mu = 4$, $\tau_{0\,(10.6)} = 0.445$ (1.91) (*2*), $a_m = 2.0$, $\mu = 4$, $\tau_{0\,(10.6)} = 0.814$ (2.95) (*3*), $a_m = 2.5$, $\mu = 5$, $\tau_{0\,(10.6)} = 1.413$ (4.27) (*4*) and $a_m = 3.0$, $\mu = 5$, $\tau_{0\,(10.6)} = 2.80$ (6.57) (*5*); the similarity parameters are $N_{v0} \approx 0.24$, $F = 59.1 \gg 1$ and $N_T = 0.00924$, 0.0159, 0.0279, 0.0562, and 0.106 for points (*1–5*), respectively.

Table 5. Transparency of the medium at the distance of the exponential radius $\mathrm{Tr}_{10.6}(r_0) = I(x = r_0, z = L)/I(r_0, 0), \mathrm{Tr}_{0.57}(r_0)$ at the wavelengths 10.6 and 0.57 μm, respectively. Variations in the optical thickness of the aerosol layer $\Delta\tau_{10.6}/\tau_0, \Delta\tau_{0.57}/\tau_0$ in the stationary limit under experimental conditions [1, 15] for $P_0 = 800$ W, $\tau_0 = 1.413$ ($\tau_{0.57} = 4.27$), $N_T = 0.0562$, $N_p = 2.30 \times 10^{-2}$, $N_{v0} = 0.238$, 0.5, 1 ($r_0 = 0.02$, 0.0289, 0.0409 m, $V_0 = 0.30$, 0.0994, 0.0351 m s^{-1}).

N_{v0}	$\mathrm{Tr}_{10.6}(r_0)$	$\mathrm{Tr}_{0.57}(r_0)$	$\Delta\tau_{10.6}/\tau_0$	$\Delta\tau_{0.57}/\tau_0$
0.238	0.231	0.0586	0.513	0.360
0.5	0.523	0.1699	0.798	0.613
1	0.811	0.3870	0.934	0.791

5. Conclusions

We considered the basic physical characteristics and similarity parameters of the nonstationary process of clearing a small dispersive water aerosol with a laser beam. Such a problem was solved earlier by using a simplifying assumption of the quasi-stationary temperature $\mathrm{d}T/\mathrm{d}t \approx 0$ [1, 2]. We have shown that the result substantially depends on the clearing parameter N_{v0}, the thermal self-action parameter N_T, the optical thickness parameter N_β (or τ_0), and the parameter N_p of the relative pressure of saturated vapour.

It has been demonstrated that the transparency of the clearing medium can be considerably increased by increasing the parameter N_{v0} at the constant power of a rectangular pulse by changing the beam radius and the flow velocity of the medium.

The results of calculations and experimental data are in good agreement.

References

1. Volkovitskii O.A., Sedunov Yu.S., Semenov L.P. *Rasprostranenie intensivnogo lazernogo izlucheniya v oblakakh* (Propagation of Intense Laser Radiation in Clouds) (Leningrad: Gidrometeoizdat, 1982).
2. Zuev V.E., Zemlyanov A.A., Kopytin Yu.D., Kuzikovskii A.V. *High-power Laser Radiation in Atmospheric Aerosols* (Amsterdam: D. Reidel, 1985; Novosibirsk: Nauka, 1984).
3. Kucherov A.N. *Kvantovaya Elektron.*, **22**, 253 (1995) [*Quantum Electron.*, **25**, 236 (1995)].
4. Prokhorov A.M. (Ed.) *Spravochnik po lazeram* (Handbook of Lasers) (Moscow: Sov. Radio, 1978) Vol. 2; Pressley R.J. (Ed.) *Hanbook of Lasers with Selected Data on Optical Technology* (Cleveland: Chemical Rubber Co., 1971).
5. Boreisho A.S. *Kvantovaya Elektron.*, **35**, 393 (2005) [*Quantum Electron.*, **35**, 393 (2005)].
6. Mazin I.P., Khrgian A.H. (Eds) *Oblaka i oblachnaya atmosfera. Spravochnik* (Handbook on Clouds and Cloudy Atmosphere) (Leningrad: Gidrometeoizdat, 1989).
7. Bohren C.F., Huffman D.R. *Absorption and Scattering of Light by Small Particles* (New York: Wiley, 1983; Moscow: Mir, 1986).
8. Kucherov A.N. *Teplofiz. Vys. Temp.*, **29**, 144 (1991) [*High Temperature*, **29**, 135 (1991)].
9. Vinogradova M.B., Rudenko O.V., Sukhorukov A.P. *Teoriya voln* (Theory of Waves) (Moscow: Nauka, 1979).
10. Knight J. *AIAA J.*, **17**(5), 519 (1979).
11. Fleck J.A. Jr., Morris J.R., Feit M.D. *Appl. Phys.*, **10** (2), 129 (1976).
12. McCormack. *AIAA Paper*, No. 69-354 (1969).
13. Peyret R., Taylor T. *Computational Methods for Fluid Flow* (Berlin: Springer, 1983).
14. Kucherov A.N. *Intern. J. Heat and Mass Transfer*, **43** (15), 2793 (2000).
15. Volkovitskii O.A., Mamonov V.K. *Kvantovaya Elektron.*, **4**, 1123 (1977) [*Sov. J. Quantum Electron.*, **7**, 634 (1977)].